ISBN: 978-981-18-5852-9
WCSE 2022 Spring Event: 2022 9th International Conference on Industrial Engineering and Applications
doi: 10.18178/wcse.2022.04.058

Liver Tumor Motion Estimation Based on Respiration-Induced Skin Change Using Principal Component Analysis and Nearest Neighbor Method

Jie Zhang[1,2 +]

[1] The Cancer Hospital of the University of Chinese Academy of Sciences (Zhejiang Cancer Hospital), Hangzhou, China

[2] Institute of Basic Medicine and Cancer (IBMC), Chinese Academy of Sciences, Hangzhou, China

Abstract. This paper proposes a liver tumor motion tracking approach based on respiration-induced skin change by using principal component analysis (PCA) and nearest neighbor estimation (NNE). The proposed method is abbreviated as PCA-NNE and is developed on the NNE in our previous work. The PCA-NNE and NNE are both estimation models by correlating internal target motion and its external surrogate. Their difference is that the surrogate for NNE is the marker attached on skin, while for PCA-NNE, the surrogate is the entire skin change. In PCA-NNE, PCA derives several principal components (PCs) from skin, and then the PCs were inputted into NNE to estimate target motion. Through this way, PCA-NNE simplify the selection of surrogate. Similar to NNE, PCA-NNE needs data to construct patient-specific model before application. To evaluate PCA-NNE, we use a digital torso phantom to create abdominal computed tomography (CT) images of a virtual patient. By setting different breathing parameters and locations of a lesion, we simulated 21 sets of respiration-correlated CT with a length of nearly 1 minutes, and derived synchronized liver tumor motion and skin change from them. For each set, the data during the first 2 ~ 3 respiration periods were used for modeling. The remaining data were used for evaluation. Two metrics were adopted for assessment. The root-mean-square error (RMSE) was used to validate its accuracy. The estimation time per sample (t) was used to evaluate its real-time performance. The results showed a RMSE of < 3mm and a t of < 15ms for all evaluation datasets. It suggested a good precision and real-time performance for PCA-NNE.

Keywords: liver tumor motion tracking based on surface, nearest neighbor estimation, principal component analysis

1. Introduction

By delivering high-dose x-ray to a target region, radiation treatment kills malignant cells and protects neighboring normal tissues. Therefore, accurate tumor location is critical in radiotherapy. Caused by breathing, liver motion ranges from 5mm to 50mm[1-3]. It affects target coverage and treatment effectiveness adversely. To compensate this motion, estimating the internal target from external signal (called surrogate) is a potential solution[4-6].

Linear regression[7-9] is the most common mathematical representation between target motion and surrogate data. Before modelling phase, the synchronized target and surrogate data are captured. The parameters of the regression formula are determined optimally based on these training data. During application, the linear model gives an estimated target position by inputting a measured surrogate. Similarly, B‐spline smoothing[10] and support vector regression[11-13] are also reported. These approaches use an explicit function to describe the correlation between target and surrogate. It's easy to lose efficacy, since the correspondence between them isn't constant.

Cyberknife[14] is a well-known system which achieves tumor motion tracking. Its target motion estimation model is a linear, quadratic, or constrained fourth order polynomial one[15]. During treatment, the real-time location of the internal tumor can be estimated by the external markers using the above polynomial models. Since the correlation between internal target and external surrogate is likely to change with the time

+ Corresponding author.
E-mail address: zhangjienju@sina.com; zhangjie@zjcc.org.cn.

passing, the model parameters need a periodical update to adapt to the gradual change of the correspondence. To achieve it, the internal target position is acquired by an additional X-ray imaging, and then is correlated with the newly detected external markers. Through this way, Cyberknife guarantees the model accuracy, but additional non-therapeutic X-ray exposure is added to the patients.

In the previous work[16], we proposed a nearest neighbor estimation (NNE) based model to generate real-time internal target position by feeding external surface marker motion. Different with the aforementioned models, NNE doesn't adopt an explicit mathematical function as a correlation. It is proved effective when breathing pattern changes, such as coughing, sneezing, harrumphing, and speaking. In NNE, the external marker position has an influence on the estimation accuracy. An approach to simplify the selection of the external surrogates is needed to improve NNE.

In this context, we proposed a model whose input is the entire skin in the abdominal region, rather than several markers. The proposed model adopts principal component analysis (PCA) to derive several principal components (PCs) from the changing skin, and then inputs them into the above NNE model to give an estimated target location. The proposed method substitutes the PCs for the external markers in NNE, and the PCs are automatically derived from the skin. It omits the step of attaching markers on patients.

In this paper, the proposed model is abbreviated as PCA-NNE. To validate it, we used a digital torso phantom to simulate the liver tumor motion and its corresponding skin change. Then we applied our model on these simulated data to assess its precision and time cost per estimation. The PCA-NNE and its evaluation experiment are detailed in section 2. The results are presented and discussed in section 3 and 4 respectively. The conclusion was given in section 5.

2. Materials and Methods

2.1. The PCA-NNE Method

Similar to the NNE[16], the PCA-NNE consists of modelling and estimation phases.

In the modelling phase, we get one-to-one mapping set $\{(\boldsymbol{f}_i, \boldsymbol{v}_i)|i=1, 2, \ldots, N\}$. Wherein, $\boldsymbol{f}_i$ means the surface obtained at ith sampling time. It is composed of three-dimension (3D) positions of all surface points. $\boldsymbol{v}_i$ represents the target's 3D locations at ith sampling time. We use PCA to derive PCs (denoted as $\{\boldsymbol{u}_i \mid i=1, 2, \ldots, N\}$) from $\{\boldsymbol{f}_i \mid i=1, 2, \ldots, N\}$, and get its corresponding project matrix $\boldsymbol{W}$. The $\boldsymbol{u}_i$ encompasses $3\times M$ values which relate to M PCs along each axis of three dimensions. Then the one-to-one mapping set is written as $\Psi:=\{(\boldsymbol{u}_i, \boldsymbol{v}_i) \mid i=1, 2, \ldots, N\}$ and then falls back into the scope of the NNE method[16].

During estimation phase, when detecting a current surface $\boldsymbol{f}_j$, we apply $\boldsymbol{W}$ on it to get corresponding PCs (denoted as $\boldsymbol{u}_j$). Then the current target location is estimated as:

(a) rule 1: if $\boldsymbol{u}_j$ is within the range of $\boldsymbol{u}_i$, we search for its K nearest neighbors (denoted as $\boldsymbol{u}_t$) in Ψ. The estimated current target location $\tilde{\boldsymbol{v}}_j$ equals to the average of K target positions ($\boldsymbol{v}_t$):

$$\tilde{\boldsymbol{v}}_j = \frac{1}{K}\sum_{t=1}^{K}\boldsymbol{v}_t \tag{1}$$

in which $\boldsymbol{v}_t$ corresponds to $\boldsymbol{u}_t$. The nearest neighbor is determined using the shorter Euclidean distance between $\boldsymbol{u}_j$ and all $\boldsymbol{u}_i$s. The Euclidean distance is also used in the nearest neighbor searching in the following two rules.

(b) rule 2: if $\boldsymbol{u}_j$ is outside the range of $\boldsymbol{u}_i$, but its previous one $\boldsymbol{u}_{j-1}$ is in the range, we search for K nearest neighbors (denoted as $\boldsymbol{u}_{t-1}$) of $\boldsymbol{u}_{j-1}$. Then

$$\tilde{\boldsymbol{v}}_j = \frac{1}{K}\sum_{t=1}^{K}\boldsymbol{v}_t \tag{2}$$

where $\boldsymbol{v}_t$ corresponds to $\boldsymbol{u}_t$. $\boldsymbol{u}_t$ is the PCs at next sampling time of $\boldsymbol{u}_{t-1}$.

(c) rule 3: if $\boldsymbol{u}_j$ and $\boldsymbol{u}_{j-1}$ both go outside the range of $\boldsymbol{u}_i$, we would construct a new one-to-one set Ψ' and search for nearest neighbors in the new set.

The new set is $\Psi':=\{(\boldsymbol{u}'_i, \boldsymbol{v}_i) \mid i=1, 2, \ldots, N\}$. Firstly, we decompose $[\boldsymbol{u}_1, \boldsymbol{u}_2, \ldots, \boldsymbol{u}_N]^{\mathrm{T}}$ using singular value

decomposition (SVD) and get its right singular vectors $\boldsymbol{r}$. From $\boldsymbol{r}$, we ignore the vector with the minimum singular value, and then obtain the new vectors $\boldsymbol{r}'$. By applying $\boldsymbol{r}'$ on $\boldsymbol{u}_i$ and $\boldsymbol{u}_j$, $\boldsymbol{u}'_i$ and $\boldsymbol{u}'_j$ are generated. Subsequently, we search for $\boldsymbol{u}'_j$'s K nearest neighbors (denoted as $\boldsymbol{u}'_t$) in Ψ' and

$$\tilde{\boldsymbol{v}}_j = \frac{1}{K}\sum_{t=1}^{K}\boldsymbol{v}_t \tag{3}$$

in which $\boldsymbol{v}_t$ corresponds to $\boldsymbol{u}'_t$.

In this paper, K=2 and M=4. The value determination of K and M is elaborated in Discussion.

2.2. Simulated Data Using a Digital Torso Phantom

The digital torso phantom is four-dimension (4D) extended cardiac-torso phantom (XCAT)[17] which is developed by Duke University. The lesion function in XCAT can model spherical lesions in a virtual body at any location. By setting breathing parameters (e.g., respiration period and diaphragm amplitude), XCAT can produce a series of respiration-correlated computed tomography (RCCT) images of a virtual patient.

In this work, we simulated 21 sets of RCCT with a respiration period of 4s ~ 6s and a diaphragm amplitude of 15mm ~ 20mm. The spherical lesions in the liver were set at three different locations (indicated by lesion No.1, 2 and 3 in Table 1). These RCCT images had a length of nearly 1 minutes and a sampling frequency of 1.6Hz ~ 5Hz. From the RCCT, we derived the synchronized target and surface data using threshold segmentation.

The details of the simulated data were listed in Table 1.

Table 1. Details of the simulated data.

dataset No.	lesion No.	respiration period (s)	sampling frequency (Hz)	diaphragm amplitude (mm)
1	1	5	2.00	20
2		4	2.50	20
3		5	3.20	15
4		6	1.67	20
5		4	2.50	15
6		6	1.67	15
7		5.2	5	20
8	2	5	2.00	20
9		4	2.50	20
10		5	3.20	15
11		6	1.67	20
12		4	2.50	15
13		6	1.67	15
14		5.2	5	20
15	3	5	2.00	20
16		4	2.50	20
17		5	3.20	15
18		6	1.67	20
19		4	2.50	15
20		6	1.67	15
21		5.2	5	20

2.3. Validation Experiment

The simulated data was split into two sets for modelling and evaluation. The data during the first 2 ~ 3 respiration periods (8s ~ 18s) were used for modeling. The rest data were used for evaluation.

The root-mean-square error (RMSE) and time per estimation (t) were used to assess the PCA-NNE. RMSE is calculated as:

$$RMSE = \sqrt{\frac{1}{L}\sum e_j^2} \tag{4}$$

where $e_j = \left\| \tilde{\boldsymbol{v}}_j - \boldsymbol{v}_j \right\|$ is the estimation error at jth sampling time. $\tilde{\boldsymbol{v}}_j$ is the estimated target position and $\boldsymbol{v}_j$ is the true one. $\| \|$ means the Euclidean distance. L is the amount of data in estimation phase.

The motion range (r) of the spherical lesion during evaluation phase was provided for comparison with RMSE. It is used to further assess the precision of PCA-NNE. In a case that r is significantly larger than RMSE, it means that the proposed PCA-NNE is capable of achieving good estimation. Otherwise, the low RMSE may come from the low r, and thus the PCA-NNE doesn't reach the desirable precision.

To know more about the results, we adopted the percentiles of e_j. Specially, they are the median (denoted as $e^{(50)}$), 75th percentile (denoted as $e^{(75)}$), 95th percentile (denoted as $e^{(95)}$) and 99th percentile (denoted as $e^{(99)}$).

3. Results

The results were plotted in Fig 1. The statistics of the estimation errors were summarized in Table 2.

Fig. 1 suggests that all evaluation sets have a RMSE of < 3mm and a t of < 15ms. The target motion range of > 14mm tells that the low RMSE doesn't come from a low motion range, and the PCA-NNE is effective.

Table 2 tells us that all datasets have an $e^{(75)}$ of < 4mm and most of them achieve $e^{(75)}$ of < 3mm. Among the all datasets, eight sets have an $e^{(95)}$ of > 5mm and fourteen sets have an $e^{(99)}$ of > 5mm. In this context, we set 5mm as the clinically acceptable maximum error, since a margin of 5mm is usually expanded from the clinical tumor volume (CTV) to planning tumor volume (PTV) to account for the positioning error[18]. These errors of > 5mm would be further analysed in Discussion.

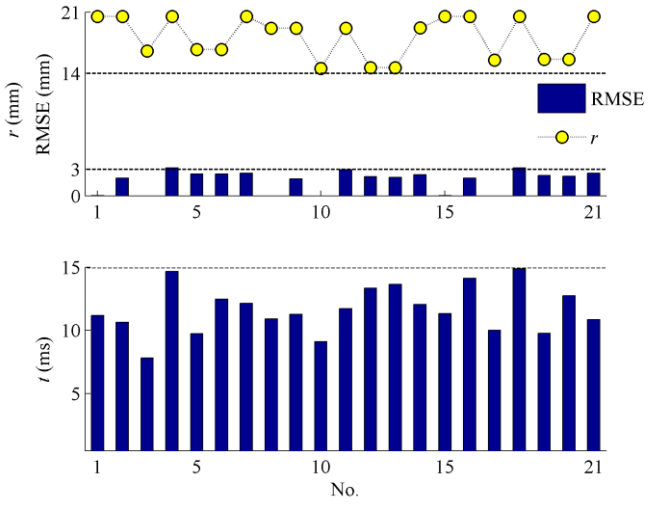

Fig. 1. Illustration of the evaluation results. RMSE is the estimation error. r is the target motion range. t is time per estimation.

Table 2. Estimation error's statistics of the results

dataset No.	$e^{(50)}$ mm	$e^{(75)}$ mm	$e^{(95)}$ mm [a]	$e^{(99)}$ mm [a]
1	0.00	0.00	0.02	0.02
2	0.64	2.15	4.09	**5.10**
3	0.00	0.00	0.00	0.00
4	3.36	3.98	**5.35**	**6.33**
5	0.76	2.73	**6.23**	**6.59**
6	1.33	3.07	4.96	**5.91**
7	0.62	2.68	**6.01**	**7.65**
8	0.00	0.00	0.00	0.00
9	0.53	2.35	3.81	4.63
10	0.00	0.00	0.00	0.00
11	2.96	3.75	4.96	**5.99**
12	0.70	2.56	**5.15**	**5.25**
13	1.25	2.45	3.90	**5.08**
14	0.61	2.53	**5.66**	**7.15**
15	0.00	0.00	0.02	0.02
16	0.64	2.15	4.09	**5.10**
17	0.00	0.00	0.00	0.00
18	3.36	3.98	**5.35**	**6.33**
19	0.76	2.74	**5.53**	**5.75**
20	1.33	2.68	4.20	**5.38**
21	0.62	2.68	**6.01**	**7.65**

[a.] The values of >5mm are printed in bold.

4. Discussion

In this section, we give a discussion on the validation results of the proposed PCA-NNE in subsection 4.1, the details on the parameter setting of PCA-NNE in subsection 4.2, and further analysis on the estimation error of larger than 5mm in subsection 4.3.

4.1 Discussion on the PCA-NNE Performance

This paper proposed a PCA-NNE approach which is developed based on our NNE method[16] to track liver tumor motion. For PCA-NNE, the external surrogate is the respiration-induced skin change, while the NNE method adopts the markers attached on skin as the surrogates. Through this way, PCA-NNE simplify the selection of surrogates, since the locations of external markers in NNE have an influence on the estimation accuracy.

Fig. 1 shows a good precision of PCA-NNE, because all validation datasets had a RMSE of < 3mm. The estimation time (t) of <15ms for one sample suggests a good real-time performance of PCA-NNE.

The modelling length of 8s ~ 18s is the duration of 2 ~ 3 breathing periods for each dataset. The test length is 42s ~ 52s. It illustrates that the PCA-NNE can achieve a good estimation accuracy even with a relatively fewer modelling data. In clinical application, a comparatively short modelling time can reduce the discomfort of patients.

4.2 Parameter Setting of the PCA-NNE

There are two parameters in the PCA-NNE which may affect the accuracy and time cost of the method. They are the number of nearest neighbors (denoted as K) and the number of PCs derived from the changing skin (denoted as M).

The value setting of K is correlated with the length of modeling data. K is supposed not to be larger than the number of respiration periods in the modeling data. It is because that the NNE was proposed based on an assumption that the whole respiration system in a human being is a continuous one. Therefore, when an external surrogate appears at a nearby location where it travelled to in the past time, its corresponding target is high likely to go to a position where the target showed up at that past time.

Since the modeling length in this experiment is 2 ~ 3 respiration periods, it is reasonable to infer that the number of the nearby locations where the target travelled in the past time is 2~3 too. Therefore, K was set as 2 in this context. The $K = 3$ can't be used for the dataset with a modeling duration of 2 breathing periods. $K = 2$ nearest neighbors can be searched for the dataset with a modeling duration of 3 breathing periods.

The value of M was set by validation. As stated in Section 2, the mapping set Ψ is one-to-one. Because the target position ($\boldsymbol{v}_i$) in Ψ is 3D, the number of dimensions of $\boldsymbol{u}_i$ (i.e., $3\times M$) is supposed not to be less than 3. Through this way, the mapping relationship between $\boldsymbol{u}_i$ and $\boldsymbol{v}_i$ is possible to be one-to-one.

During the validation, we found that the estimation accuracy wasn't better with a higher M. The reason may be that a higher M introduces more irrelevant information into the PCA-NNE. The irrelevant information works as noise in the estimation approach, and hence deteriorates the precision. Besides, a higher M involves more data in the search of nearest neighbors. Accordingly, it would increase the time cost for one estimation.

A lower M doesn't relate to a higher estimation precision either. It is because that a fewer PCs may fold the mapping space between 3D motion of the internal target and external surrogates. Accordingly, the mapping relationship in Ψ may not be one-to-one any more.

In the future work, we will conduct more studies on the parameter setting and its influence on the performance of PCA-NNE.

4.3 Analysis on the Estimation Error of > 5mm

The estimation error of > 5mm results from the inadequate description of target and surrogate motion space during modelling phase.

As shown in Table 1, the sampling frequencies are 1.6Hz ~ 5Hz. By multiplying sampling frequency with its corresponding respiration period, we know that there are 10 ~ 26 samples in a breathing cycle. The distance between two neighboring target samples can be inferred to be around 1.5mm ~ 4mm. It is estimated as

$$\text{distance between neighboring target samples} = \frac{\text{disphragm amplitude}}{\text{sample amount in a breathing cycle} \div 2}$$

Therefore, the K (K=2 in this context) nearest neighbors of target searched by the PCA-NNE may have a deviation of $\leq$ 1.5mm ~ 4mm to the true position of the current target. The deviation eventually causes the estimation error. Note that the above deduction is based on the assumption that the motion shifts of target and of diaphragm are 1:1. In fact, the motion shift ratio may be larger than 1:1. Thus, the distance between two neighboring target samples during modeling is likely to be larger than 1.5mm ~ 4mm, and finally causes an estimation error of > 5mm.

To tackle it, involving more samples with a lower time interval in the modelling phase is a potential solution. Specifically, we can use a medical imaging system with a high imaging frequency, such as ultrasonography, to acquire the internal target motion for modelling. Or the interpolation, constructing new samples based on the known data, can be adopted to reduce the time interval between samples and hence increase the sample size in the modelling duration.

5. Conclusion

This work proposed a PCA-NNE method to track liver tumor motion. The PCA-NNE estimates the internal target motion by correlating it with the respiration-induced skin change. This method was validated on a digital torso phantom which can produce a series of a virtual patient's RCCT scans. These scans'

breathing and lesion parameters can be determined by customer. The assessment results show a good accuracy and a real-time performance of PCA-NNE. Besides, it can reduce the discomfort of patients by accepting a relatively fewer modeling data and thus promising in clinical practice.

6. Acknowledgements

This work was supported by Zhejiang Provincial Natural Science Foundation of China (LQ20H180016) and National Natural Science Foundation of China (82001928).

7. References

[1] Davies, S., A. Hill, R. Holmes, et al., Ultrasound quantitation of respiratory organ motion in the upper abdomen. 1994. 67(803): 1096-1102.

[2] Balter, J.M., L.A. Dawson, S. Kazanjian, et al., Determination of ventilatory liver movement via radiographic evaluation of diaphragm position. 2001. 51(1): 267-270.

[3] Suramo, I., M. Päivänsalo, and V. Myllylä, Cranio-caudal movements of the liver, pancreas and kidneys in respiration. 1984. 25(2): 129-131.

[4] Ehrhardt, J. and C. Lorenz, 4D modeling and estimation of respiratory motion for radiation therapy. 2013.

[5] Remy, C., D. Ahumada, A. Labine, et al., Potential of a probabilistic framework for target prediction from surrogate respiratory motion during lung radiotherapy. 2021. 66(10): 105002.

[6] Savanovic, M., B. Strbac, D. Jaros, et al., Assessment of internal and external surrogates for lung stereotactic body radiation therapy. 2021. 18(5): 352-360.

[7] Fahmi, S., F.F. Simonis, and M. Abayazid, Respiratory motion estimation of the liver with abdominal motion as a surrogate. 2018. 14(6): e1940.

[8] Chen, B., N. Weber, F. Odille, et al., Design and validation of a novel MR-compatible sensor for respiratory motion modeling and correction. 2016. 64(1): 123-133.

[9] Willmann, J., B. Sidiqi, C. Wang, et al., Four-Dimensional Computed Tomography-Based Correlation of Respiratory Motion of Lung Tumors With Implanted Fiducials and an External Surrogate. 2022. 7(3): 100885.

[10] Buerger, C., R.E. Clough, A.P. King, et al., Nonrigid motion modeling of the liver from 3-D undersampled self-gated golden-radial phase encoded MRI. 2012. 31(3): 805-815.

[11] Ernst, F., V. Martens, S. Schlichting, et al. Correlating chest surface motion to motion of the liver using ε-SVR–a porcine study. in International conference on medical image computing and computer-assisted intervention. 2009. Springer.

[12] Zhang, J., X. Bai, and G. Shan. Comparison of Two Different Kernel Functions of Support Vector Regression for Tracking Tumor Motion: Radial Basis Function and Linear Function. in Proceedings of the 2019 6th International Conference on Bioinformatics Research and Applications. 2019.

[13] Wang, G., Z. Li, G. Li, et al., Real-time liver tracking algorithm based on LSTM and SVR networks for use in surface-guided radiation therapy. 2021. 16(1): 1-12.

[14] Lo K M Y, Wu V W C, Li Y, et al. Factors affecting target motion in stereotactic body radiotherapy of liver cancer using CyberKnife[J]. Journal of Medical Imaging and Radiation Oncology, 2020, 64(3): 408-413.

[15] Kilby W, Dooley J R, Kuduvalli G, et al. The CyberKnife® robotic radiosurgery system in 2010[J]. Technology in cancer research & treatment, 2010, 9(5): 433-452.

[16] Zhang, J., X. Huang, Y. Shen, et al., Nearest neighbor method to estimate internal target for real-time tumor tracking. 2018. 17: 1533033818786597.

[17] Segars, W.P., G. Sturgeon, S. Mendonca, et al., 4D XCAT phantom for multimodality imaging research. 2010. 37(9): 4902-4915.

[18] Paik EK, Kim MS, Choi CW, et al. Dosimetric comparison of volumetric modulated arc therapy with robotic stereotactic radiation therapy in hepatocellular carcinoma. Radiat Oncol J. 2015;33 (3):233-241